DOI: 10.1021/cg900313b

CRYSTAL GROWTH & DESIGN
Communication
2009, Vol. 9
4230–4234

Hierarchical Al_2O_3 Nanobelts and Nanowires: Morphology Control and Growth Mechanism

Yong Zhang,[†] Ruying Li,[†] Xiaorong Zhou,[§] Mei Cai,[⊥] and Xueliang Sun*,[†]

[†]*Department of Mechanical and Materials Engineering, University of Western Ontario, London, Ontario, Canada, N6A 5B9,* [§]*School of Materials, The University of Manchester, Manchester, M60 1QD, U.K., and* [⊥]*General Motors Research and Development Center, Warren, Michigan 48090-9055*

Received March 17, 2009; Revised Manuscript Received July 31, 2009

ABSTRACT: We report here a tunable synthesis of single crystalline hierarchical α-Al_2O_3 nanobelts and nanowires by selectively applying a vapor−liquid−solid (VLS) and vapor−solid (VS) strategy in a chemical vapor process. The resultant nanostructures were characterized by scanning electron microscopy, transmission electron microscopy, high-resolution transmission electron microscopy, energy dispersive X-ray spectroscopy, and X-ray powder diffraction. The hierarchical nanobelts were generated by a noncatalytic oriented growth of Al_2O_3 vertical to the {110} planes enclosed with {001} and {100} planes following a VS mode. The hierarchical nanowires were obtained through a catalytic growth in a VLS process. This well-controlled synthesis strategy is expected to be applicable to fabrication of other hierarchical nanobelts or nanowires.

One-dimensional (1D) nanostructured material, as a well-defined building block, plays an important role in constructing nanoscaled smart systems.[1] As high density interconnects,[2] hierarchical 1D nanostructures that possess a distinct trunk-branch feature have been recently developed and can be used in various nanodevices such as optical,[3] opto-electronic,[4] electronic,[5] gas-sensing,[6] energy scavenging devices,[7] fuel cells,[8] and solar cells.[9] It is known that the development of hierarchical 1D nanostructures with improved properties depends not only on the alternation of electronic states by creating interfacial regions,[10] but also on their morphological arrangement, shape, and crystallographic orientation.[11] Therefore, research toward morphology and structure control of complex 1D nanostructures has attracted more and more attention.

Alumina is a well-studied traditional structure material with valuable applications in photoluminescence,[12] dielectric response,[13] and selective catalysis.[14] Doubtlessly, tailored hierarchical 1D alumina nanostructures are promising for the realization of multifunctional nanodevices. In addition, excellent mechanical properties and thermal stability of alumina promise their unique applications in nanodevices under extreme conditions such as high temperature.

The growth of α-Al_2O_3 nanowires and nanobelts has been reported previously.[15] Recently, cantaloupe-like and microspherical hierarchical γ-Al_2O_3 nanostructures have been synthesized by low temperature wet chemical routes.[16] However, there have been few reports on hierarchical 1D alumina nanostructures up to now. Vapor−liquid−solid (VLS) and vapor−solid (VS) mechanisms are two commonly recognized modes in dominating the growth of 1D nanostructures. In this study, VLS and VS modes have been selectively applied to produce hierarchical alumina nanobelts and nanowires in well-controlled chemical vapor deposition (CVD) processes, respectively. The hierarchical nanobelts were generated by a noncatalytic oriented growth following a VS mode, while the hierarchical nanowires were obtained through a catalytic growth in a VLS process. Interestingly, transmission electron microscopy reveals that the second-generation nanobelts keep an angle of 60° with the longitudinal axis of the first-generation nanobelt. The second-generation nanowires are almost perpendicular to the longitudinal axis of the first-generation nanowires. The correlations between the first- and the second-generation nanostructures as well as their growth mechanisms are discussed.

Experimental Procedures. A vacuum free hot-wall chemical vapor deposition (HWCVD) system[15e] was employed to synthesize the hierarchical alumina nanostructures. Figure 1 demonstrates the schematic diagram of the setup.

An alumina tube (outer diameter, 2 in., length: 48 in.) was mounted horizontally inside the furnace, where temperature and gas flow rate were controlled. Hierarchical alumina nanobelts were synthesized at 1350 °C using a mixture of aluminum and alumina powder (weight ratio: 4:1) as the starting materials. Hierarchical alumina nanowires were obtained at 1250 °C using a mixture of aluminum, alumina, and tin (weight ratio: 4:1:0.2) as the starting materials. An alumina plate was put onto the top of the alumina boat to collect the product. High-purity argon (99.999%) was passed through the tube at a rate of 400 sccm (standard cubic centimeters per minute) for 30 min to purge oxygen from the furnace before the furnace was heated to target temperatures. Then, the temperature was kept for 1 h with argon gas being flowed through the reaction chamber. The reaction chamber was finally cooled to room temperature under flowing argon gas.

The synthesized products were examined initially by using a Hitachi S-4500 field emission scanning electron microscope (FESEM). Further characterization of the 1-D nanostructures was carried out using a Rigaku-MiniFlex powder X-ray diffraction spectrometer (XRD), a JEOL 2010 transmission electron microscope (TEM) equipped with energy dispersive X-ray (EDX) analysis capability, and a Tecnai G^2 F30 high-resolution transmission electron microscope (HRTEM).

Results and Discussion. Figure 2a shows the SEM image of the nanostructures prepared at 1350 °C. A large amount of hierarchical wire-like features was observed. A close examination of the SEM image revealed that the wire-like features are composed of two generations of nanobelts, as shown in Figure 2b,c. Our SEM observations indicate the oblong geometric cross-section of the first-generation nanobelt. Interestingly, it can be seen that the angles between the second-generation nanobelts and the first-generation nanobelts are kept constant at approximately 60°. No particles are observed at the tip of the second-generation nanobelt, indicating a VS growth mechanism of the nanobelts.[17] Figure 2d shows the XRD pattern of the nanobelts. The diffraction peaks can be well assigned for a rhombohedral structure of α-Al_2O_3 with $R\bar{3}c$ (167) symmetry (based on JCPDS Card No: 46-1212).

*To whom correspondence should be addressed. E-mail: xsun@eng.uwo.ca. Phone: +1 519 661 2111 ext 87759. Fax: +1 519 661 3020.

 Published on Web 09/02/2009

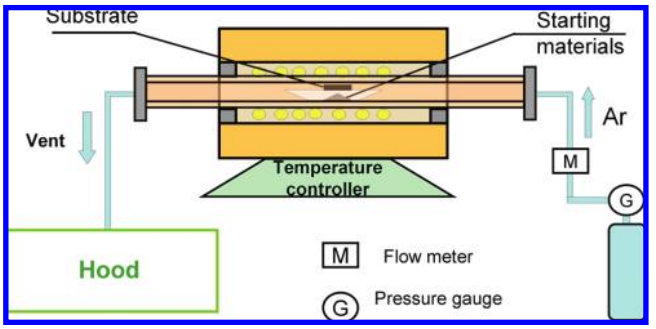

Figure 1. Schematic diagram of the setup for growing hierarchical Al_2O_3 nanobelts and nanowires.

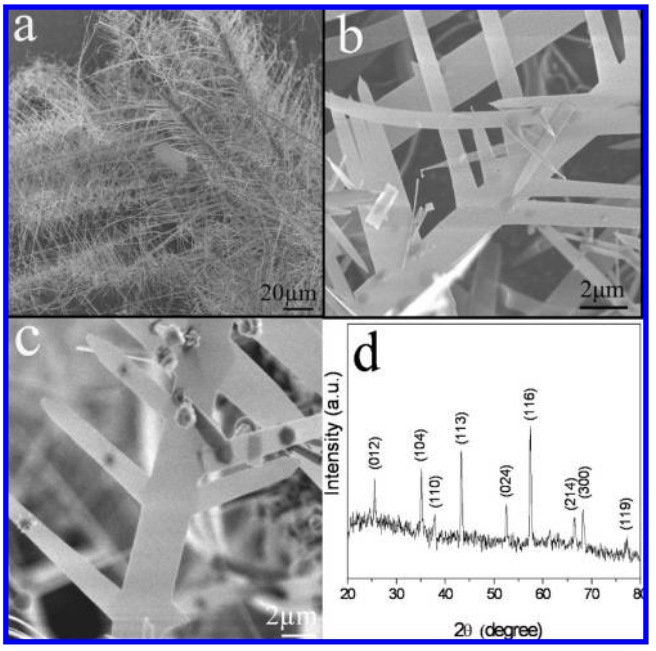

Figure 2. (a) Low magnification, (b) and (c) high magnification SEM images, and (d) XRD pattern of the hierarchical Al_2O_3 nanobelts.

Figure 3a shows the SEM images of the product synthesized at 1250 °C with addition of a tin source, revealing hierarchical nanowires. SEM observations reveal a square or nearly round geometric cross-section of the first-generation nanowire. Again, the XRD pattern of the nanowire can be indexed as α-Al_2O_3 (Figure 3b). Increased magnification image of Figure 3c shows nearly perpendicular growth of the second-generation nanowires on the first generation ones. In addition, fine particles are evident at the tip of each second-generation nanowire. The observation of the hierarchical nanowires along the longitudinal axis exhibits an aligned growth of the second-generation nanowires on the first-generation ones, as shown in Figure 2d. TEM observations provide more detailed morphological and structural information of the resultant nanostructures.

TEM images of a typical nanobelt are shown in Figure 4, confirming the hierarchical structure of the nanobelt. It is clearly evident that a hierarchical nanostructure is composed of the first-generation nanobelt trunk and the second-generation nanobelt branches. All second-generation nanobelt branches grow in directions with an angle of 60° or 120° to the first-generation nanobelt trunk, as indicated in Figure 4a. Figure 4b shows an increased magnification TEM image of the hierarchical nanobelt. Although these nanobelts have complex shapes, their quasi-single crystal structure is confirmed by selected area electron diffraction.

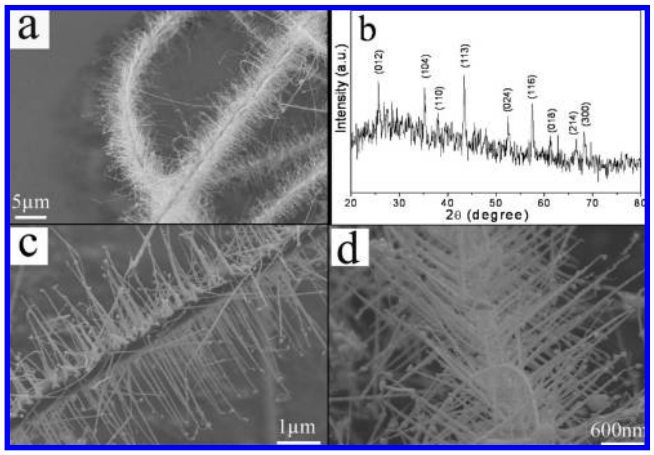

Figure 3. (a) A low magnification SEM image, (b) XRD pattern, (c) and (d) high magnification SEM images of the hierarchical Al_2O_3 nanowires.

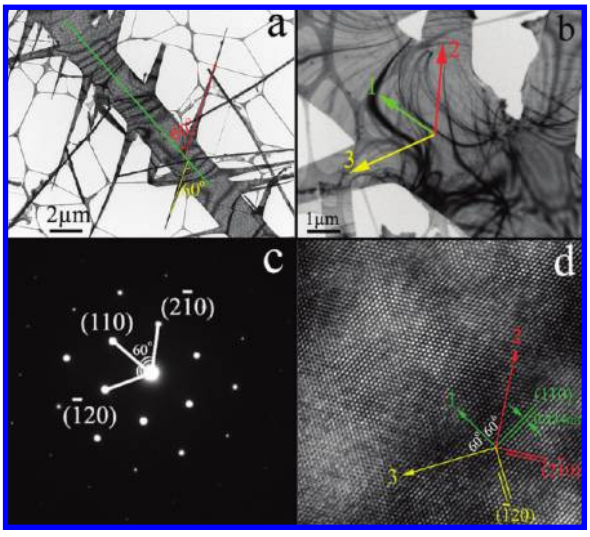

Figure 4. Panels (a) and (b) bright field TEM images, (c) selected area electron diffraction pattern, (d) high resolution TEM image, of the hierarchical Al_2O_3 nanobelts.

Diffraction patterns have been taken from the trunk nanobelt, branch nanobelt, and interface between the trunk and branch nanobelts, with the incident electron beam along the [001] zone axis, revealing a single crystal, as shown in Figure 4c. By using a three-index notation (Miller indices), the spots are indexed as (110), (2$\bar{1}$0), (1$\bar{2}$0) planes of α-Al_2O_3, which are (11$\bar{2}$0), (2$\bar{1}$1$\bar{0}$), and (1$\bar{2}$1$\bar{0}$) planes in a four-index notation system (Miller-Bravais indices). These three planes are actually equivalent crystallographic planes in a hexagonal unit cell of α-Al_2O_3 since there is a 6-fold symmetry around the *c*-axis, which will be illustrated later in Figure 6. These three crystal planes all belong to the family of {110} planes.

As indicated in Figure 4b, the growth direction of the trunk nanobelt is perpendicular to the (110) plane, while that of the two nanobelt branches is perpendicular to (2$\bar{1}$0) and (1$\bar{2}$0) plane, respectively. In addition, the angles of (110)/(2$\bar{1}$0) and (110)/(1$\bar{2}$0) are both 60°, which is consistent with the measured angles between the nanobelt trunk and the nanobelt branches from SEM and TEM images of Figures 2 and 4. Figure 4d shows high resolution lattice fringes of the nanobelt. The spacing of the lattice fringes is measured as around 0.234 nm, consistent with the *d* value of the {110} crystal plane of α-Al_2O_3. As demonstrated in Figure 4d, the lattice fringes can be assigned to the (110), (2$\bar{1}$0),

and ($\bar{1}$20) plane, respectively, confirming that the growth of the two generation nanobelts in Figure 4b is achieved through the atoms stacking along the direction perpendicular to the (110), (2$\bar{1}$0), and ($\bar{1}$20) plane, respectively. TEM image of Figure 5a shows a typical hierarchical nanostructure of two-generation hierarchical Al_2O_3 nanowires. Unlike the growth of the nanobelts, the branched nanowires were grown in the direction perpendicular to the trunk nanowire. In addition, particles can be observed at the tip of each branch nanowire. Figure 5b shows the EDX spectrum taken from a particle at the nanowire tip. Sn was detected along with Al, O, and Cu. Copper yields are from the TEM copper grid. The presence of tin particles at the tips of nanowires indicates tin-catalytic growth of the nanowires, that is, the VLS growth mechanism of the nanowires. Selected area electron diffraction with the incident electron beam along the [001] zone axis indicates that the branched nanowires are single crystalline, as shown in Figure 5c. The diffraction pattern can be indexed as α-Al_2O_3. The growth direction of the branched nanowire is vertical to the (110) plane. As shown in Figure 5d, the HRTEM image shows that the spacing between sets of parallel fringes in the length direction of the branch nanowire is about 0.237 nm, equal to the *d* value of {110} planes of α-Al_2O_3.

We have performed a series of experiments to control the morphology of the nanostructures. We found that the morphology control of 1D Al_2O_3 nanostructures is a complex process. Several growth parameters, such as growth temperature, amount of the starting materials (ASM), and usage of catalyst, are primary factors in determining the product morphology. Generally speaking, small ASM and low temperature favored the growth of regular nanowires.[15e] The two-generation hierarchical nanobelts can be produced at increased ASM and higher temperature without catalyst. While catalyst was applied, greater ASM favored the growth of two-generation hierarchical nanowires. Although two-generation hierarchical nanowires could also be obtained without using catalyst, following the VS growth mechanism, the product was a mixture of two-generation hierarchical nanowires with regular nanowires and nanobelts. The employment of tin as catalyst ensured identical morphology of two-generation hierarchical nanowires in the product. Detailed dependence of the product morphology on the growth parameters is demonstrated in Table 1; the experimental conditions marked with "▼" means the involved parameters.

To further control the growth of hierarchical nanobelts and nanowires, it is essential to get insight into their growth mechanism. For the growth process from aluminum and alumina powder to 1D alumina nanostructures, the involved reactions have been discussed previously.[15e] In this case, the reaction between the alumina and aluminum powder generates a volatile alumina suboxide (Al_2O) vapor,[18] which reacts with oxygen and results in the formation of the hierarchical nanobelts and nanowires. There are probably three sources which provide the oxygen in the synthesis: (1) the argon gas (99.999% purity), which contains a small amount of oxygen with the partial pressure of 10^{-5} atm,[19] (2) residue oxygen in the reaction chamber after the purge, and (3) possible air leakage. Figure 6a,b schematically demonstrates the growth processes of the two-generation hierarchical nanobelts and nanowires, respectively.

The growth of the two-generation hierarchical nanobelts is likely governed by the VS mechanism, while the production of the two-generation hierarchical nanowires follows the VLS mechanism. Nucleation and growth are two essential steps during the growth of nanostructures. The growth of the two-generation hierarchical nanobelts can be regarded as the two-dimensional nucleation and atom stacking along certain crystallographic directions in a VS growth process.[17] It has been theoretically established that the possibility of two-dimensional nucleation is related to surface energy of the crystal, temperature, and supersaturated ratio of vapor based on the following equation:[20]

$$P_N = B \exp\left(-\frac{\pi\sigma^2}{K^2 T^2 \ln \alpha}\right)$$

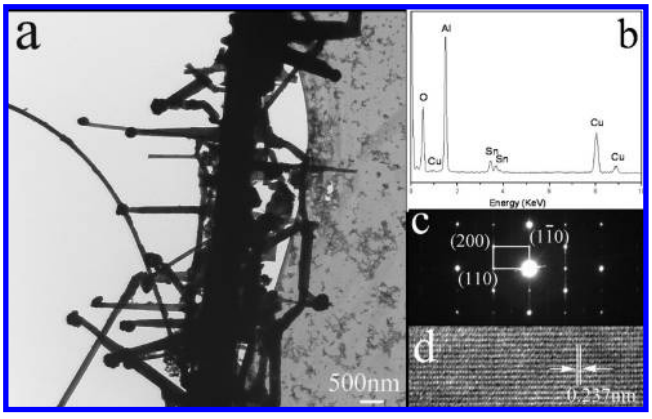

Figure 5. Panel (a) bright field TEM image, (b) EDX spectrum of the nanowire tip with the catalyst particle (c) selected area electron diffraction pattern, (d) high resolution TEM image, of the hierarchical Al_2O_3 nanowire.

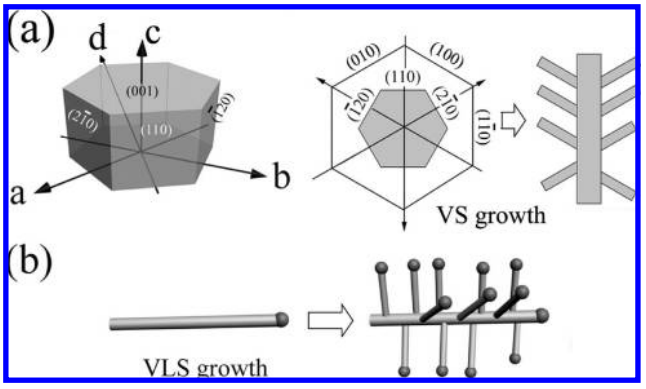

Figure 6. Schematic diagram of (a) a hexagonal Al_2O_3 cell unit and growth of the hierarchical Al_2O_3 nanobelts via the VS mechanism, (b) growth of the hierarchical Al_2O_3 nanowires via the VLS mechanism.

Table 1. Morphology Dependence of the Product on the Growth Parameters

involved experimental parameters						
temperature (°C)		amount of the starting materials (mg)		catalyst		
1350	1250	500	200	with Sn	no Sn	morphology of the product
▼		▼			▼	two generation nanobelts
	▼	▼		▼		two generation nanowires
▼		▼		▼		two generation nanobelts and two generation nanowires
	▼	▼			▼	two generation nanowires, regular nanowires and nanobelts
▼			▼	▼		regular nanowires and nanobelts
▼			▼		▼	regular nanowires and nanobelts
	▼		▼	▼		regular nanowires (diameter is more uniform)
	▼		▼		▼	regular nanowires (diameter is less uniform)

where P_N is the nucleation possibility, B is a constant, σ is surface energy, K is the Boltzmann constant, T is growth temperature, and α is the supersaturation ratio of the vapor. According to the equation, two-dimensional (2D) growth of crystal is preferentially enclosed by low index crystal planes. Figure 6a shows a hexagonal unit cell of α-Al_2O_3, indicating that the growth direction of the trunk nanobelt and branch nanobelts is vertical to the {110} planes, and enclosed by ± (001) planes at the top and bottom plane of a hexagonal unit cell, and by {100} planes at the lateral plane of each nanobelt. While the critical value of temperature and vapor supersaturation ratio is achieved, growth of two-generation hierarchical nanobelts is triggered.

On the basis of SEM and TEM observations, solidified spherical droplets were observed at the tips of the nanowires, which is commonly considered to be evidence for the VLS growth mechanism. At the reaction temperature, aluminum and tin vapor were generated by thermal evaporation from the molten aluminum−tin alloy. In this case, Al−Sn−O eutectic liquid droplets were formed on the surface of the alumina substrate,[21] providing energetically favored sites for condensation and absorption of aluminum and oxygen species from the vapor phase. While the central axial wire grew quickly with the catalyst particle at the tip, smaller alloy droplets could be formed on the axial nanowire surface, which leads to the growth of the second-generation nanowires. Therefore, we propose that the growth of the hierarchical Al_2O_3 nanowires can be separated into two stages, as shown in Figure 6b. The first stage was a fast growth of the Al_2O_3 trunk nanowire with the eutectic alloy liquid as the catalyst; the second stage of the growth was the nucleation and epitaxial growth of the branch due to the aggregation of the vapor onto the trunk Al_2O_3 nanowire surface. It should be mentioned that it still remains unclear why the second-generation nanowires are perpendicular to the first-generation nanowire, instead of keeping a 60° angle with the longitudinal axis of the first-generation nanowire as the two-generation nanobelts growth. For aligned growth of nanowires dominated by a VS mechanism, there is always a crystallographic relationship between nanowires and the substrate. Similar to the two-generation nanobelts growth in our work, the nucleation of the second-generation nanostructure occurs following an epitaxial growth mode along certain crystallographic planes of the first-generation nanostructure, and the growth orientation of the second-generation nanostructure is related to surface energy of the crystal, temperature, supersaturated ratio of vapor, and so on. For vertically aligned growth of nanowires via a VLS growth mechanism, however, there is not necessarily a crystallographic relationship between the nanowires and the substrate. We propose two possible reasons to explain why the second-generation nanowires are perpendicular to the first-generation nanowire: (1) when the liquid catalyst is formed on the surface of the first-generation nanowire, the catalyst droplet may dissolve the surface of the first-generation nanowire and creates some degree of surface roughness, which offers larger interfacial area for noncrystallographic nucleation. In this case, the nucleation of the second-generation nanowires proceeds vertically to the catalyst/first-generation nanowire interface and the growth direction is confined by the catalyst, which is similar to the case described in the literature;[22] (2) the other possibility is that vertical growth of the nanowires are obtained due to the epitaxial growth of the second-generation nanowires on lattice-matched first-generation nanowire, similar to the case in the previous report.[23] In this case, the growth direction of the first-generation nanowire is perpendicular to that of the second-generation nanowires in crystallography. Further work is underway.

Conclusion. In conclusion, we have developed a well-controlled synthesis route via chemical vapor deposition under ambient pressure to fabricate hierarchical Al_2O_3 nanobelts and nanowires. The hierarchical Al_2O_3 nanobelts are obtained through the oriented growth of Al_2O_3 vertical to the {110} planes enclosed with {001} and {100} planes following a VS growth model. The second-generation nanobelts keep an angle of 60° with the longitudinal axis of the first generation nanobelt. The growth of the hierarchical Al_2O_3 nanowires can be achieved by introducing tin as the catalyst in a VLS process. The second-generation nanowires are almost perpendicular to the longitudinal axis of the first-generation nanowires. On the condition that temperature and supersaturation ratio of vapor are carefully controlled, the growth strategy proposed in this report is expected to be applicable to the growth of other hierarchical nanobelts and nanowires, which is essential in constructing various nanodevices with complex structures.

Acknowledgment. This research was supported by General Motors of Canada, the Natural Science and Engineering Research Council of Canada (NSERC), Canada Research Chair (CRC) Program, Canadian Foundation for Innovation (CFI), Ontario Research Fund (ORF), Early Researcher Award (ERA), and the University of Western Ontario. We thank David Tweddell, Fred Pearson for fruitful discussion, structural characterization, and special support.

References

(1) (a) Ajayan, P. M. *Chem. Rev*. **1999**, *99*, 1787. (b) Xia, Y. N.; Yang, P. D.; Sun, Y. G.; Wu, Y. Y.; Mayers, B.; Gates, B.; Yin, Y. D.; Kim, F.; Yan, Y. Q. *Adv. Mater*. **2003**, *15*, 353.
(2) (a) Wang, D. L.; Qian, F.; Yang, C.; Zhong, Z. H.; Lieber, C. M. *Nano Lett*. **2004**, *4*, 871. (b) Teo, B. K.; Sun, X. H. *Chem. Rev*. **2007**, *107*, 1454.
(3) (a) Yan, H. Q.; He, R. H.; Johnson, J.; Law, M.; Saykally, R. J.; Yang, P. D. *J. Am. Chem. Soc*. **2003**, *125*, 4728. (b) Dick, K. A.; Deppert, K.; Larsson, M. W.; Mårtensson, T.; Seifert, W.; Wallenberg, L. R.; Samuelson, L. *Nat. Mater*. **2004**, *3*, 380. (c) Shen, G. Z.; Lee, C. J. *Cryst. Growth Des*. **2005**, *5*, 1085. (d) Pan, Z. W.; Mahurin, S. M.; Dai, S.; Lowndes, D. H. *Nano Lett*. **2005**, *5*, 723. (e) Wang, H.; Zhang, X. H.; Meng, X. M.; Zhou, S. M.; Wu, S. K.; Shi, W. S.; Lee, S. T. *Angew. Chem., Int. Ed*. **2005**, *44*, 6934.
(4) (a) Jiang, Y.; Zhang, W. J.; Jie, J. S.; Meng, X. M.; Zapien, J. A.; Lee, S. T. *Adv. Mater*. **2006**, *18*, 1527. (b) Sun, S. H.; Meng, G. W.; Zhang, G. X.; Zhang, L. D. *Cryst. Growth Des*. **2007**, *7*, 1988.
(5) (a) Suyatin, D. B.; Sun, J.; Fuhrer, A.; Wallin, D.; Froberg, L. E.; Karlsson, L. S.; Maximov, Ivan.; Wallenberg, L. R.; Samuelson, L.; Xu, H. Q. *Nano Lett*. **2008**, *8*, 1100. (b) Kuan, C. Y.; Hon, M. H..; Chou, J. M.; Leu, I. C. *Cryst. Growth Des*. **2009**, *9* (2), 813.
(6) Ponzoni, A.; Comini, E.; Sberveglieri, G.; Zhou, J.; Deng, S. Z.; Xu, N. S.; Ding, Y.; Wang, Z. L. *Appl. Phys. Lett*. **2006**, *88*, 203101.
(7) Qin, Y.; Wang, X. D.; Wang, Z. L. *Nature* **2008**, *451*, 809.
(8) Sun, X; Li, R.; Stansfield, B.; Dodelet, J. P.; Désilets, S. *Chem. Phys. Lett*. **2004**, *394*, 266.
(9) Xu, L. F.; Chen, Q. W.; Xu, D. S. *J. Phys. Chem. C* **2007**, *111*, 11560.
(10) Gudiksen, M. S.; Lauhon, L. J.; Wang, J.; Smith, D. C.; Lieber, C. M. *Nature* **2002**, *415*, 617.
(11) Bell, A. T. *Science* **2003**, *299*, 1688.
(12) (a) Li, T.; Yang, S. G.; Du, Y. W. *Nanotechnology* **2005**, *16*, 365. (b) Fang, X. S.; Ye, C. H.; Peng, X. S.; Wang, Y. H.; Wu, Y. C.; Zhang, L. D. *J. Mater. Chem*. **2003**, *13*, 3040.
(13) Fang, X. S.; Ye, C. H.; Zhang, L. D.; Xie, T. *Adv. Mater*. **2005**, *17*, 1661.
(14) Zhu, H. Y.; Riches, J. D.; Barry, J. C. *Chem. Mater*. **2002**, *14*, 2086.
(15) (a) Jin, Y. Z.; Zhu, Y. Q.; Brigatti, K.; Kroto, H. W.; Walton, D. R. M. *Appl. Phys. A: Mater. Sci. Process*. **2003**, *77*, 113. (b) Wu, N. F.; Chen, H. J.; Chueh, Y. L.; Lin, S. J.; Lin, L. J.; Hsu, W. K. *Chem. Commun*. **2005**, *2*, 204. (c) Peng, X. S.; Zhang, L. D.; Meng, G. W. et al. *J. Phys. Chem. B* **2002**, *106*, 11163. (d) Zhao, Q.; Xu, X.; Zhang, H.; Chen, Y.; Xu, J.; Yu, D. *Appl. Phys. A: Mater. Sci. Process*. **2004**, *79*, 1721. (e) Zhang, Y.; Li, R. Y.; Zhou, X. R.; Cai, M.; Sun, X. L. *J. Nanomater*. **2008**, 250370.
(16) (a) Feng, Y. L.; Lu, W. C.; Zhang, L. M.; Bao, X. H.; Yue, B. H.; Lv, Y.; Shang, X. F. *Cryst. Growth Des*. **2008**, *8*, 1426. (b) Zhang, L.; Zhu, Y. J. *J. Phys. Chem. C* **2008**, *112*, 16764.
(17) Wang, Z. L. *J. Nanosci. Nanotechnol*. **2008**, *8*, 27.

(18) Brewer, L.; Searcy, A. W. *J. Am. Chem. Soc.* **1951**, *73*, 5308.
(19) Lu, F. H.; Chen, H. Y. *Thin Solid Films* **1999**, *355*−*356*, 374.
(20) Dai, Z. R.; Pan, Z. W.; Wang, Z. L. *Adv. Funct. Mater.* **2003**, *13*, 9.
(21) Morgan, P. E. D.; Housley, R. M. *J. Am. Ceram. Soc.* **1995**, *78*, 263.
(22) Chung, H. S.; Jung, Y. W.; Zimmerman, T. J.; Lee, S. H.; Kim, J. W.; Lee, S. H.; Kim, S. C.; Oh, K. H.; Agarwal, R. *Nano Lett.* **2008**, *8*, 1328.
(23) Martensson, T.; Svensson, C. P.; Wacaser, B. A.; Larsson, M. W.; Seifert, W.; Deppert, K.; Gustafsson, A.; Wallenberg, L. R.; Samuelson, L. *Nano Lett.* **2004**, *4*, 1987.